Observation of high-spin oblate band structures in ^{141}Pm

L. Gu (顾龙),[1] S. J. Zhu (朱胜江),[1,*] J. G. Wang (王建国),[1] E. Y. Yeoh (杨韵颐),[1] Z. G. Xiao (肖志刚),[1]
S. Q. Zhang (张双全),[2] J. Meng (孟杰),[2] M. Zhang (张明),[1] Y. Liu (刘宇),[1] H. B. Ding (丁怀博),[1] Q. Xu (徐强),[1]
L. H. Zhu (竺礼华),[3] X. G. Wu (吴晓光),[3] C. Y. He (贺创业),[3] G. S. Li (李广生),[3] L. L. Wang (王烈林),[3]
Y. Zheng (郑云),[3] and B. Zhang (张彪)[3]
[1]*Department of Physics, Tsinghua University, Beijing 100084, People's Republic of China*
[2]*Department of Technical Physics, Peking University, Beijing 100871, People's Republic of China*
[3]*China Institute of Atomic Energy, Beijing 102413, People's Republic of China*
(Received 17 April 2011; published 6 June 2011)

The high-spin states of ^{141}Pm have been investigated through the reaction ^{126}Te(^{19}F,4n) at a beam energy of 90 MeV. A previous level scheme has been updated with spins up to $49/2\hbar$. Six collective bands at high spins are newly observed. Based on the systematic comparison, one band is proposed as a decoupled band; two bands with strong $\Delta I = 1$ $M1$ transitions inside the bands are suggested as the oblate bands with $\gamma \sim -60^\circ$; three other bands with large signature splitting have been proposed with the oblate-triaxial deformation with $\gamma \sim -90^\circ$. The triaxial n-particle-n-hole particle rotor model calculations for one of the oblate bands in ^{141}Pm are in good agreement with the experimental data. The other characteristics for these bands have been discussed.

DOI: 10.1103/PhysRevC.83.064303 PACS number(s): 21.10.Re, 23.20.Lv, 27.60.+j, 25.70.Jj

I. INTRODUCTION

The rare earth nuclei in $A \sim 140$ region with the neutron number approaching the $N = 82$ closed shell show strong shape driving effects at high-spin states. According to the crank shell model (CSM) calculations [1], the alignment of the proton of lower $h_{11/2}$ orbits will drive the nucleus toward a prolate shape ($\gamma \sim 0^\circ$) while the alignment of the neutron of upper $h_{11/2}$ orbits tends to drive the nucleus toward an oblate shape ($\gamma \sim -60^\circ$) in the Lund convention [2]. In previous reports, many oblate bands have been observed in this region, such as in ^{131}La [1], ^{136}La [3], ^{137}Ce [4], ^{138}Pr [5], ^{139}Nd [6], and ^{140}Pm [7]. Such observed oblate bands just indicate the strong neutron shape driving effect in this region.

For $N = 80$ isotones in this region, nuclei are expected with small quadrupole deformation and the level structures will show significant quasiparticle characters at low spins. However, at the high-spin states, the collective oblate bands were also observed in ^{137}La [8] and ^{138}Ce [9], besides the superdeformed bands observed in ^{142}Sm [10] and ^{143}Eu [11]. For ^{141}Pm, some level structures have been reported from β-decay and heavy-ion nuclear reactions in early reports [12–14], and then were reinvestigated with ^{133}Cs(^{12}C,4n) reactions [15]. However, in contrast to the neighboring nuclei, the information of the high-spin states in ^{141}Pm is still lacking and no collective band in this nucleus was identified. In this paper, we report on the reinvestigation of the high-spin states of ^{141}Pm. The level scheme has been expanded and many collective bands at high-spin states have been observed.

II. EXPERIMENT AND RESULTS

High-spin states of ^{141}Pm have been populated via ^{126}Te(^{19}F,4n) fusion-evaporation reactions at a beam energy of 90 MeV which was obtained by the HI-13 tandem accelerator at the China Institute of Atomic Energy (CIAE). The target of 2.85 mg/cm^2 thick enriched ^{126}Te was prepared by evaporating tellurium metal powder on a 21.75 mg/cm^2 thick gold backing. The in-beam γ−rays have been detected by twelve Compton-suppressed high-purity Ge (HPGe) detectors and one clover detector which consists of four Ge crystals. Three HPGe detectors and the clover detector were placed at around 90° and other detectors were placed at around 140° (two), 150° (two), 125° (two), 42° (two), and 65° (one) with respect to beam direction. The resolutions of the Ge detectors are between 1.8 and 2.2 keV at 1.333 MeV γ-ray energy. The relative efficiencies were calibrated using ^{152}Eu and ^{133}Ba sources. A total of 1.9×10^8 γ-γ coincidence events were collected and were sorted out into a γ-γ coincidence matrix. The γ-γ coincidence data were analyzed with the RADWARE software package [16].

A level scheme of ^{141}Pm established in the present work is shown in Fig. 1. The collective band structures have been labeled on top of the bands with the numbers (1)–(6). Three sets of cascades are also labeled with the characters (A), (B), and (C). The multipolarity of the γ transitions is determined by the directional correlation of oriented state (DCO) intensity ratios. In order to obtain the DCO ratios, an asymmetrical two-dimensional angular-correlation matrix was produced with the events collected by the detectors at around 90° along one axis and the events collected by other detectors along other axes. The γ-transition energies, relative transition intensities, DCO ratios, multipolarities, and the spin and parity (I^π) assignments are shown in Table I. The intensities of the γ transitions have been normalized to that of the 728.2 keV γ transition ($19/2^- \rightarrow 15/2^-$). As the statistic of DCO data is poorer than that in the total coincidence matrix, the DCO ratios of some weak transitions cannot be determined. Generally, a quadrupole ($\Delta I = 2$, $E2$) transition is adopted if a DCO ratio is around 0.51, and a dipole ($\Delta I = 1$) transition is assumed if a DCO ratio is around 1.01. The I^π's of the levels are assigned or

*zhushj@mail.tsinghua.edu.cn

TABLE I. The energies, relative intensities, DCO ratios, multipolarities, and spin and parity (I^π) assignments of the γ transitions and levels in ^{141}Pm.

E_γ (keV)	Intensity (%)	E_i (keV) $\rightarrow$ E_f (keV)	Assignment	R_{DCO}	Multipolarity
61.7	18.1(15)	2702.6 → 2640.9	$21/2^- \rightarrow 17/2^-$		$E2$[b]
[a]75.9	18.1(27)	3332.5 → 3256.6	$33/2^- \rightarrow 31/2^-$	1.09(8)	$M1/E2$
79.8	41.3(22)	2702.6 → 2622.8	$21/2^- \rightarrow 17/2^+$		$M2$[b]
[a]109.0	2.1(7)	5046.7 → 4937.7	$39/2^- \rightarrow 37/2^-$	0.91(15)	$M1/E2$
110.8	52.0(18)	2349.2 → 2238.4	$19/2^- \rightarrow 19/2^-$		$M1/E2$[b]
[a]139.6	6.4(8)	4861.4 → 4721.8	$31/2^- \rightarrow 29/2^-$	0.95(6)	$M1/E2$
170.3	9.3(7)	2809.9 → 2661.8	$21/2^- \rightarrow 21/2^-$		$M1$[b]
[a]175.1	6.2(8)	5512.6 → 5337.5	$(39/2^-) \rightarrow 37/2^-$		$(M1/E2)$
[a]177.9	∼43	3256.6 → 3078.7	$31/2^- \rightarrow 27/2^-$	0.48(8)	$E2$
[a]179.6	∼46	3078.7 → 2899.1	$27/2^- \rightarrow 23/2^-$	0.51(8)	$E2$
[a]180.2	9.3(6)	4514.8 → 4334.6	$37/2^- \rightarrow 35/2^-$	0.97(11)	$M1/E2$
196.5		2899.1 → 2702.6	$23/2^- \rightarrow 21/2^-$		$M1$[b]
196.9		196.9 → 0.0	$7/2^+ \rightarrow 5/2^+$		$M1$[b]
197.5		1510.2 → 1312.7	$15/2^- \rightarrow 13/2^-$		$M1/E2$[b]
[a]218.4	4.7(5)	6243.2 → 6024.8	$(41/2^-) \rightarrow (39/2^-)$	0.96(15)	$M1/E2$
218.9	9.3(9)	3465.4 → 3246.5	$25/2^- \rightarrow 25/2^-$	1.13(15)	$M1/E2$
232.6	4.2(5)	5094.0 → 4861.4	$33/2^- \rightarrow 31/2^-$	0.96(4)	$M1/E2$
[a]236.1	2.3(7)	6479.3 → 6243.2	$(43/2^-) \rightarrow (41/2^-)$	0.96(7)	$M1/E2$
236.5	18.1(11)	3701.9 → 3465.4	$25/2^- \rightarrow 25/2^-$		$M1/E2$[b]
236.6	5.7(8)	4861.4 → 4624.8	$31/2^- \rightarrow 29/2^-$	0.93(3)	$M1/E2$
243.5	7.3(7)	5337.5 → 5094.0	$37/2^- \rightarrow 33/2^-$	0.54(9)	$E2$
[a]254.7	9.0(9)	4937.7 → 4683.0	$37/2^- \rightarrow 35/2^-$	1.00(6)	$M1/E2$
[a]258.1	8.8(7)	4772.9 → 4514.8	$39/2^- \rightarrow 37/2^-$	0.94(5)	$M1/E2$
260.2	19.2(10)	2640.9 → 2380.7	$17/2^- \rightarrow 15/2^-$		$M1/E2$[b]
[a]279.9	10.1(7)	3981.8 → 3701.9	$27/2^- \rightarrow 25/2^-$	0.93(6)	$M1/E2$
291.6	4.5(5)	4916.4 → 4624.8	$31/2^- \rightarrow 29/2^-$	1.06(5)	$M1/E2$
301.0	5.7(6)	2809.9 → 2508.9	$21/2^- \rightarrow 19/2^-$	0.99(9)	$M1/E2$
312.6	30.1(13)	2661.8 → 2349.2	$21/2^- \rightarrow 19/2^-$	0.97(3)	$M1/E2$
312.9	5.5(8)	3122.8 → 2809.9	$25/2^- \rightarrow 21/2^-$	0.57(5)	$E2$
[a]312.9	2.0(7)	6792.2 → 6479.3	$(45/2^-) \rightarrow (43/2^-)$	1.02(12)	$M1/E2$
[a]313.3	3.4(5)	5407.3 → 5094.0	$35/2^- \rightarrow 33/2^-$	1.05(7)	$M1/E2$
[a]314.5	8.2(7)	5087.4 → 4772.9	$41/2^- \rightarrow 39/2^-$	0.98(6)	$M1/E2$
[a]330.2	1.0(5)	7122.4 → 6792.2	$(47/2^-) \rightarrow (45/2^-)$	0.92(23)	$M1/E2$
347.4	25.8(8)	3246.5 → 2899.1	$25/2^- \rightarrow 23/2^-$	0.93(4)	$M1/E2$
[a]353.4	∼20	2622.8 → 2349.2	$21/2^- \rightarrow 19/2^-$		$M1/E2$
[a]354.8	2.8(6)	5762.1 → 5407.3	$37/2^- \rightarrow 35/2^-$	0.94(6)	$M1/E2$
[a]355.0	3.3(6)	6353.2 → 5998.2	$45/2^- \rightarrow 43/2^-$	0.93(11)	$M1/E2$
361.3	17.1(11)	4063.2 → 3701.9	$27/2^- \rightarrow 25/2^-$	0.93(3)	$M1/E2$
[a]363.7	6.2(4)	5046.7 → 4683.0	$39/2^- \rightarrow 35/2^-$	0.55(16)	$E2$
[a]367.4	8.9(9)	4349.2 → 3981.8	$29/2^- \rightarrow 27/2^-$	0.99(8)	$M1/E2$
[a]371.7	6.7(19)	5459.1 → 5087.4	$43/2^- \rightarrow 41/2^-$	0.95(8)	$M1/E2$
[a]388.4	2.2(7)	4115.4 → 3727.0	$27/2^- \rightarrow 23/2^-$	0.37(18)	$E2$
431.6		628.5 → 196.9	$11/2^- \rightarrow 7/2^+$		$M2$[b]
[a]435.3	2.9(6)	5482.0 → 5046.7	$41/2^- \rightarrow 39/2^-$	0.99(6)	$M1/E2$
[a]442.7	5.9(4)	5901.8 → 5459.1	$45/2^- \rightarrow 43/2^-$	1.02(6)	$M1/E2$
461.0	6.9(4)	3122.8 → 2661.8	$25/2^- \rightarrow 21/2^-$	0.47(4)	$E2$
[a]461.0	3.1(6)	6814.2 → 6353.2	$47/2^- \rightarrow 45/2^-$	0.93(14)	$M1/E2$
464.2	22.8(11)	2702.6 → 2238.4	$21/2^- \rightarrow 19/2^-$	0.96(2)	$M1/E2$
[a]468.5	6.3(5)	5151.5 → 4683.0	$(37/2^-) \rightarrow 35/2^-$	1.12(7)	$(M1/E2)$
[a]469.2	7.3(5)	5094.0 → 4624.8	$33/2^- \rightarrow 29/2^-$	0.60(10)	$E2$
[a]472.1	6.2(4)	4821.3 → 4349.2	$31/2^- \rightarrow 29/2^-$	1.14(11)	$M1/E2$
486.0	12.4(12)	2622.8 → 2136.8	$17/2^+ \rightarrow 13/2^+$	0.56(5)	$E2$
496.1	12.5(11)	3157.9 → 2661.8	$23/2^- \rightarrow 21/2^-$	0.98(3)	$M1/E2$
[a]516.2	1.3(5)	5998.2 → 5482.0	$43/2^- \rightarrow 41/2^-$	1.09(12)	$M1/E2$
[a]538.9	1.0(5)	7353.1 → 6814.2	$49/2^- \rightarrow 47/2^-$	1.07(11)	$M1/E2$

TABLE I. *(Continued)*

E_γ (keV)	Intensity (%)	E_i (keV) → E_f (keV)	Assignment	R_{DCO}	Multipolarity
[a]544.3	6.3(4)	5482.0 → 4937.7	$41/2^- \to 37/2^-$	0.50(4)	$E2$
561.6	11.7(14)	4624.8 → 4063.2	$29/2^- \to 27/2^-$	1.08(4)	$M1/E2$
566.3	19.5(13)	3465.4 → 2899.1	$25/2^- \to 23/2^-$	1.03(4)	$M1/E2$
[a]578.4	5.4(4)	5399.7 → 4821.3	$33/2^- \to 31/2^-$	1.14(11)	$M1/E2$
[a]597.8	7.6(4)	4063.2 → 3465.4	$27/2^- \to 25/2^-$	1.00(5)	$M1/E2$
628.5		628.5 → 0.0	$11/2^- \to 5/2^+$		$E3$[b]
[a]628.6	9.0(7)	6402.1 → 5773.5	$43/2^- \to 39/2^-$	0.59(6)	$E2$
638.3	15.4(12)	3884.8 → 3246.5	$27/2^- \to 25/2^-$	1.08(11)	$M1/E2$
[a]646.1	17.8(11)	4916.1 → 4270.0	$35/2^- \to 31/2^-$	0.48(3)	$E2$
653.3	65.7(16)	2622.8 → 1969.5	$17/2^+ \to 15/2^+$	1.06(2)	$M1/E2$
658.6	6.1(4)	4721.8 → 4063.2	$29/2^- \to 27/2^-$	1.03(7)	$M1/E2$
[a]681.8	25.4(9)	3580.9 → 2899.1	$27/2^- \to 23/2^-$	0.45(3)	$E2$
684.2	48.8(7)	1312.7 → 628.5	$13/2^- \to 11/2^-$		$E2$[b]
[a]684.4	4.9(5)	6084.1 → 5399.7	$35/2^- \to 33/2^-$	1.03(4)	$M1/E2$
[a]689.1	21.4(10)	4270.0 → 3580.9	$31/2^- \to 27/2^-$	0.45(4)	$E2$
[a]719.0	12.1(14)	7121.1 → 6402.1	$47/2^- \to 43/2^-$	0.55(5)	$E2$
728.2	100.0(35)	2238.4 → 1510.2	$19/2^- \to 15/2^-$	0.46(1)	$E2$
777.0	112.9(47)	973.9 → 196.9	$11/2^+ \to 7/2^+$		$E2$[b]
798.2	3.7(5)	4861.4 → 4063.2	$31/2^- \to 27/2^-$	0.48(10)	$E2$
802.8	28.6(9)	3701.9 → 2899.1	$25/2^- \to 23/2^-$	1.06(4)	$M1/E2$
816.7	1.7(8)	4063.2 → 3246.5	$27/2^- \to 25/2^-$	1.04(9)	$M1/E2$
837.0	1.7(6)	4721.8 → 3884.8	$29/2^- \to 27/2^-$	1.07(10)	$M1/E2$
853.2	3.8(5)	4916.4 → 4063.2	$31/2^- \to 27/2^-$	0.47(7)	$E2$
[a]857.4	16.8(12)	5773.5 → 4916.1	$39/2^- \to 35/2^-$	0.43(5)	$E2$
[a]871.2	3.8(5)	6353.2 → 5482.0	$45/2^- \to 41/2^-$	0.52(6)	$E2$
[a]873.3	5.7(4)	6024.8 → 5151.5	$(39/2^-) \to (37/2^-)$	1.07(8)	$(M1/E2)$
881.7	207.2(38)	1510.2 → 628.5	$15/2^- \to 11/2^-$	0.45(1)	$E2$
922.9	11.0(8)	4624.8 → 3701.9	$29/2^- \to 25/2^-$	0.43(4)	$E2$
[a]924.4	6.8(4)	6697.9 → 5773.5	$43/2^- \to 39/2^-$	0.45(4)	$E2$
[a]951.5	4.2(5)	5998.2 → 5046.7	$43/2^- \to 39/2^-$	0.42(4)	$E2$
[a]953.0	4.2(8)	4075.8 → 3122.8	$(27/2^-) \to 25/2^-$	0.91(5)	$(M1/E2)$
995.6	81.5(15)	1969.5 → 973.9	$15/2^+ \to 11/2^+$	0.55(2)	$E2$
998.7	22.2(10)	2508.9 → 1510.2	$19/2^- \to 15/2^-$	0.55(3)	$E2$
[a]1002.1	10.6(14)	4334.6 → 3332.5	$35/2^- \to 33/2^-$	1.12(5)	$M1/E2$
1019.9	6.2(4)	4721.8 → 3701.9	$29/2^- \to 25/2^-$	0.60(9)	$E2$
1068.0	24.1(17)	2380.7 → 1312.7	$15/2^- \to 13/2^-$		$M1$[b]
[a]1078.0	6.3(4)	4334.6 → 3256.6	$35/2^- \to 31/2^-$	0.57(9)	$E2$
1112.6	41.8(17)	2622.8 → 1510.2	$17/2^+ \to 15/2^-$		$E1$[b]
1162.9	19.2(14)	2136.8 → 973.9	$13/2^+ \to 11/2^+$	0.91(5)	$M1/E2$
1218.6	11.3(11)	4376.5 → 3157.9	$25/2^- \to 23/2^-$	1.08(4)	$(M1/E2)$
1256.4	2.0(5)	4721.8 → 3465.4	$29/2^- \to 25/2^-$	0.49(15)	$E2$
[a]1426.4	23.8(10)	4683.0 → 3256.6	$35/2^- \to 31/2^-$	0.42(8)	$E2$
[a]1488.6	6.0(4)	3727.0 → 2238.4	$23/2^- \to 19/2^-$	0.52(7)	$E2$

[a]The γ transition identified in this work compared with the results reported in Ref. [15].
[b]The transition multipolarity taken from Ref. [15], as the DCO value for the transition can not be obtained in this work.

tentatively assigned according to the DCO ratios, the previous results, and regular level spacings.

Compared to the results reported in Ref. [15], the level scheme of ^{141}Pm has been significantly updated and expanded in the present work. Many additional levels and transitions have been identified. Six additional collective band structures (1)–(6) have been established as shown in Fig. 1. Band (1) is based on the 2899.1 keV level with spins up to $47/2\hbar$. Bands (2)–(6) are based on 3701.9, 4334.6, 5998.2, 6024.8, and 4861.4 keV levels with spins up to 35/2, 45/2, 49/2, 47/2, and $37/2\hbar$, respectively. All these bands are assigned or tentatively assigned as the odd parity bands. A total of 41 additional levels and 50 additional transitions have been identified in this work as compared with the results in Ref. [15]. As examples, here we give some coincidence γ-ray spectra in ^{141}Pm as shown in Figs. 2–5. In Fig. 2, by summing gating on the 881.7 and 728.2 keV transitions, one can see most of the corresponding coincidence γ peaks in Fig. 1. Figures 3–5 give partial coincidence spectra by gating on 857.4 [Fig. 3(a)], 472.1 [Fig. 3(b)], 1002.1 + 1078.0 [Fig. 4(a)], 516.2 + 951.5 [Fig. 4(b)], 873.3 [Fig. 5(a)], and 561.6 [Fig. 5(b)] keV transitions, respectively. In these spectra, the corresponding γ transitions inside bands

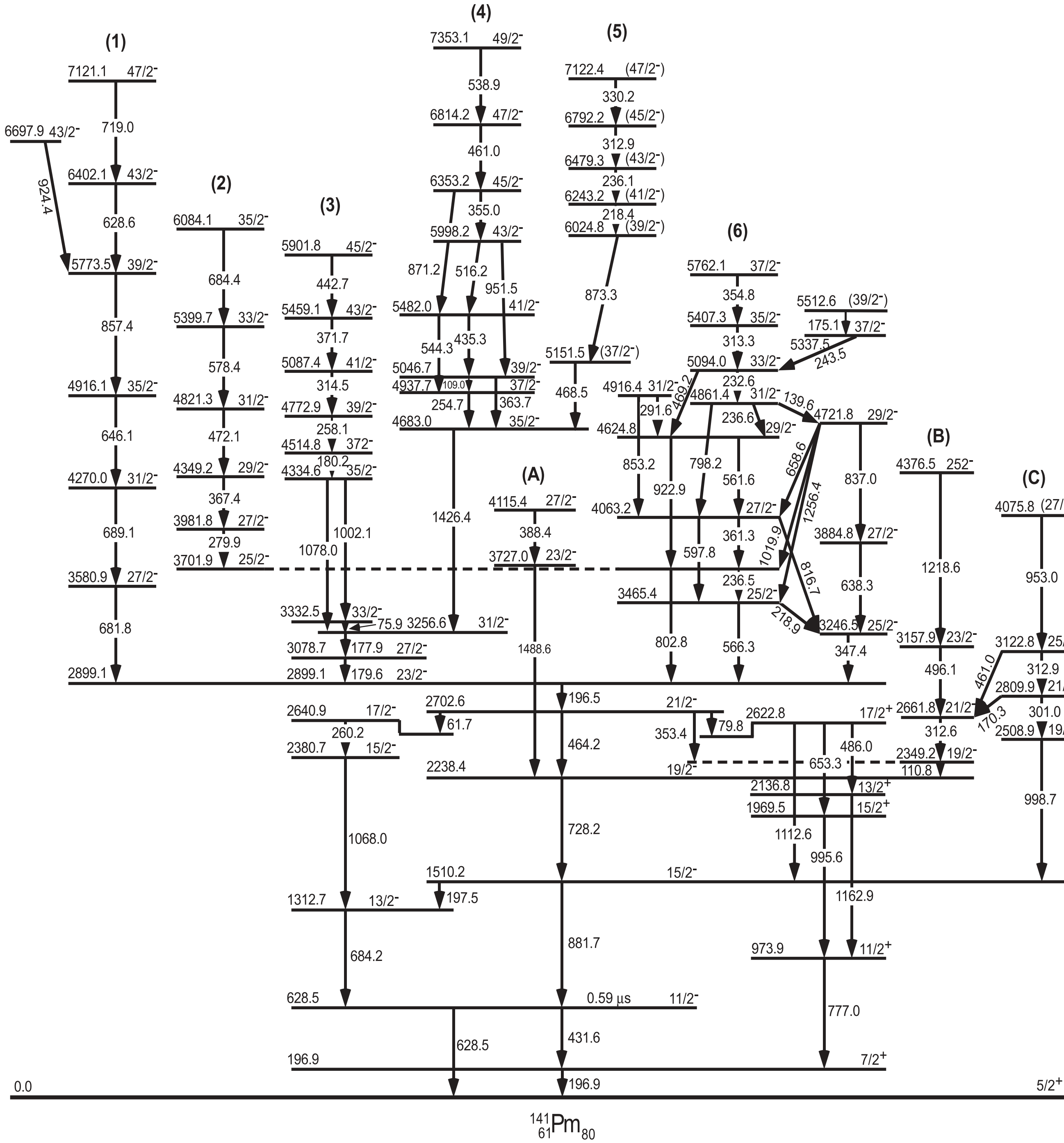

FIG. 1. The level scheme of ^{141}Pm in the present work.

(1)–(6) can be seen, such as 681.8, 689.1, 646.1, 628.6, and 719.0 keV in band (1) [shown in Fig. 3(a)]; 279.9, 367.4, 578.4, and 684.4 keV in band (2) [shown in Fig. 3(b)], 180.2 (mixed with 179.6 keV), 258.1, 314.5, 371.7, and 442.7 keV in band (3) [shown in Fig. 4(a)]; 355.0 (mixed with 353.4 keV), 461.0, and 538.9 keV in band (4) [shown in Fig. 4(b)], 218.4, 236.1, 312.9, and 330.2 keV in band (5) [shown in Fig. 5(a)]; and 232.6, 313.3, and 354.8 (mixed with 353.4 keV) keV in band (6) [shown in Fig. 5(b)]. Some other corresponding γ peaks can be seen in these spectra also.

III. DISCUSSION

From the early experiments [12], the I^{π} of the ground state in ^{141}Pm have been assigned as $5/2^{+}$. An $11/2^{-}$ isomer with 0.59 μs half-life has been observed [12,14]. Aryaeinejad *et al.* [13] and Gülmez *et al.* [14] applied the triaxial rotor plus particle model to interpret the level structures of the lower spin states. In the calculations, they assumed the triaxial oblate core of ^{140}Nd with $\beta_2 = 0.15$ and $\gamma = 34.0^{\circ}$ coupling with a valence proton. The calculated results showed that the odd

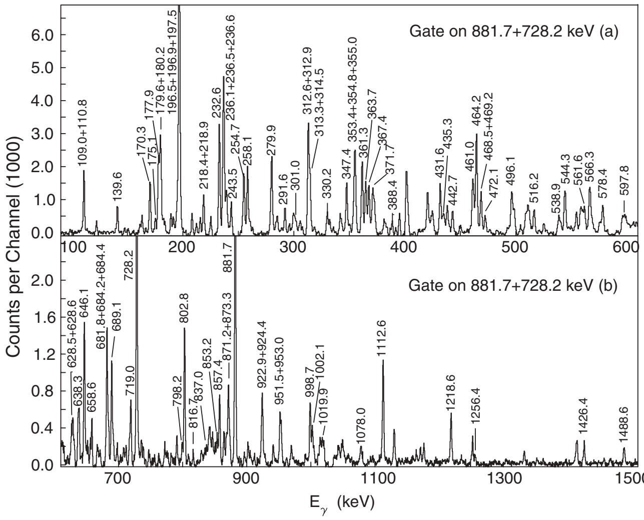

FIG. 2. The coincidence γ spectra by summing gating on 881.7 and 728.2 keV γ transitions in ^{141}Pm.

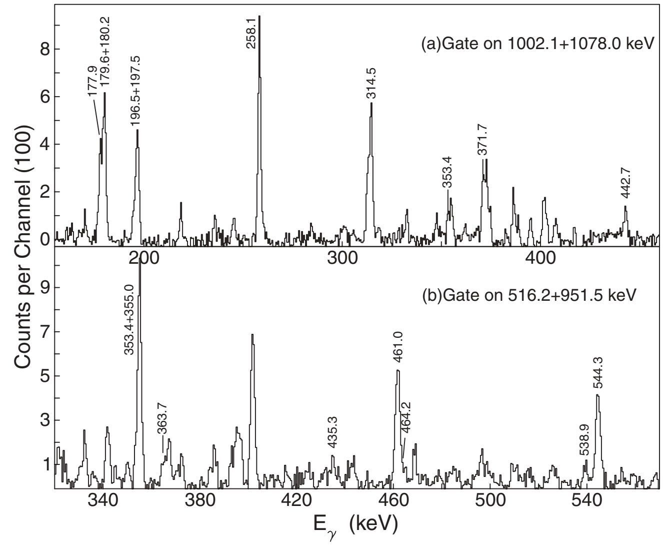

FIG. 4. The partial coincidence γ spectra by (a) summing gating on 1002.1 and 1078.0 keV and (b) summing gating on 516.2 and 951.5 keV γ transitions in ^{141}Pm.

parity levels at low-spin states in ^{141}Pm originate from $\pi h_{11/2}$ orbital coupling with the neighboring even-even core, and the even parity levels originated from $\pi d_{5/2}$ or $\pi g_{7/2}$ orbital coupling with the neighboring even-even core. In a recent publication, Bhattacharyya *et al.* [15] have made a systematic comparison for the lower spin levels in ^{141}Pm and also gave some valuable information.

As mentioned above, the high-spin collective bands (1)–(6) in ^{141}Pm are observed in this work. So in the following discussion, we will analyze the characters of these high-spin band structures.

Band (1) in ^{141}Pm, consisting of the $\Delta I = 2$ stretch $E2$ transitions, is based on the $23/2^-$ state with 2899.1 keV excited energy. This band should belong to a double decoupled band which was also observed in the neighboring odd-odd nuclei ^{134,136}Pr [17,18] and ^{138,140}Pm [7,19,20]. For double decoupled bands, only the favored signature component can be observed. According to the CSM calculation [17–20], in the configurations of these double decoupled bands, an $\Omega = 1/2$ Nilsson orbital should be included. So for the double decoupled band (1) with the odd parity in odd-A ^{141}Pm, the possible configuration may be suggested as $\pi h_{11/2} \otimes \nu(h_{11/2} \cdot f_{7/2}[541]1/2^-)$.

Bands (2) and (3) in ^{141}Pm consist of the strong $\Delta I = 1M1$ transitions without $\Delta I = 2$ $E2$ transitions inside the bands. Similar band structures have been observed in many nuclei of the $A = 130$–140 region. These bands were assigned as oblate bands with $\gamma \sim -60^\circ$. The oblate bands in this region have some remarkable characters [1,3–7,21]: (a) much stronger $\Delta I = 1$ transitions relative to $\Delta I = 2$ transitions inside the

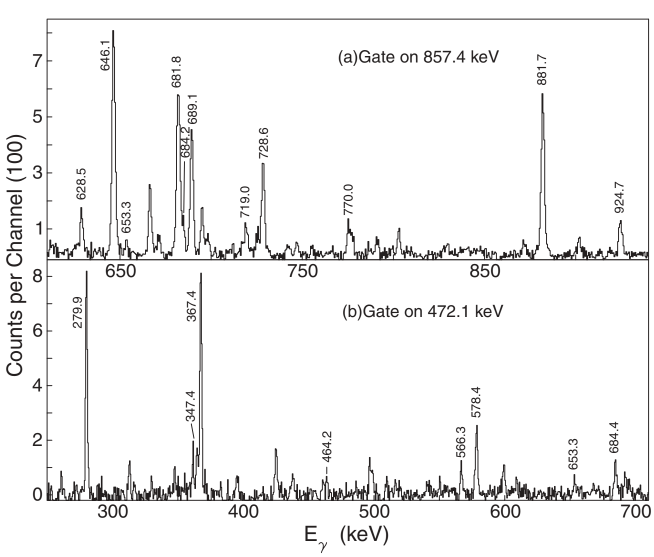

FIG. 3. The partial coincidence γ spectra by gating on (a) 857.4 and (b) 472.1 keV γ transitions in ^{141}Pm.

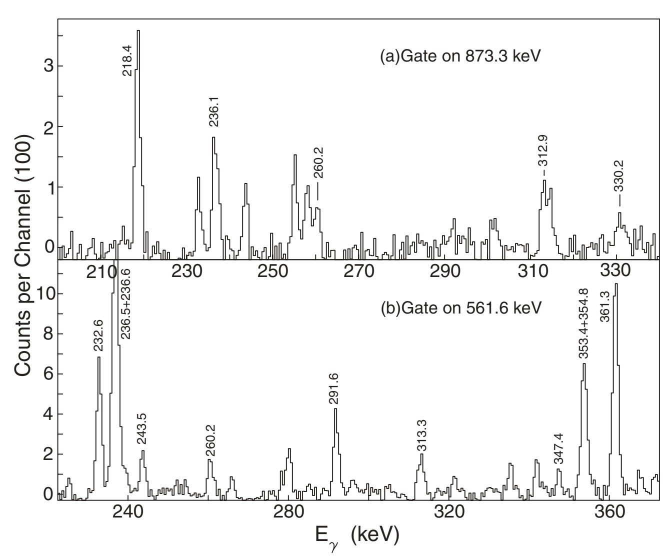

FIG. 5. The partial coincidence γ spectra by gating on (a) 873.3 and (b) 561.6 keV γ transitions in ^{141}Pm.

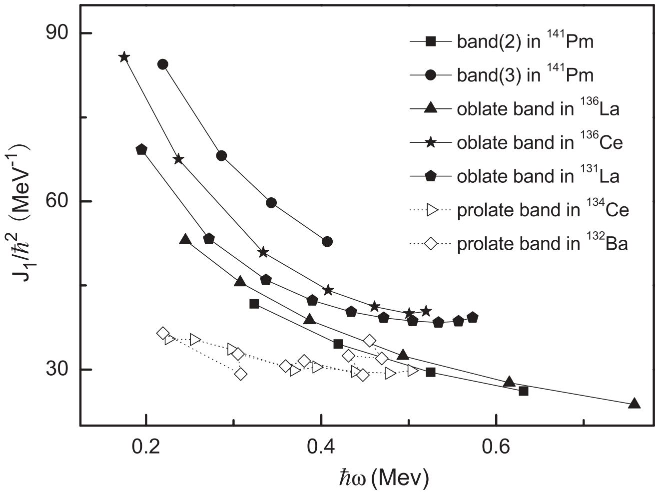

FIG. 6. Plots of the moments of inertia J_1 of bands (2) and (3) in ^{141}Pm, the oblate bands in ^{136}La, ^{136}Ce, and ^{131}La, and the prolate bands in ^{134}Ce and ^{132}Ba against the rotational frequency $\hbar\omega$.

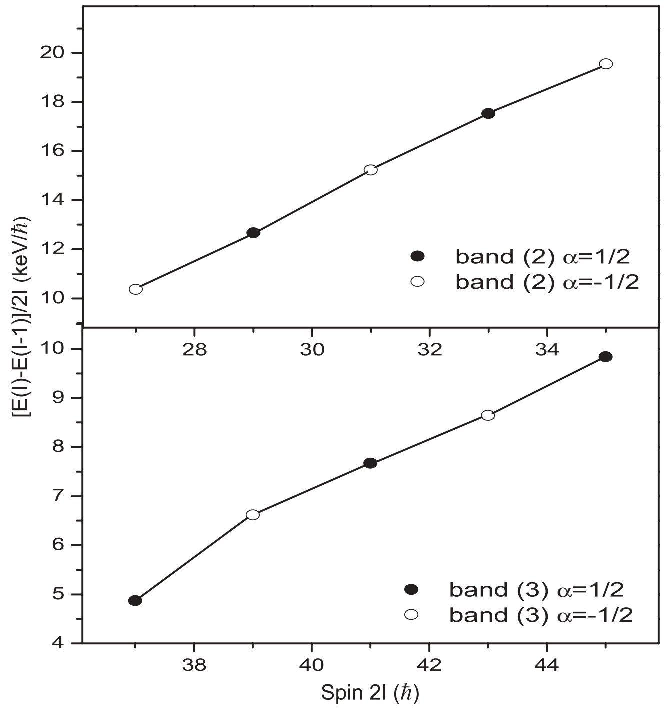

FIG. 7. Plots of the $[E(I) - E(I-1)]/2I$ vs the spin I for bands (2) and (3) in ^{141}Pm.

band, (b) different moments of inertia from those of prolate bands, and (c) no signature splitting occurrences.

Now we analyze the characteristics of bands (2) and (3) in ^{141}Pm. The experimental $B(M1; \Delta I = 1)/B(E2; \Delta I = 2)$ values in the near prolate bands are typically ~ 1 $(\mu_N/\text{eb})^2$, while values obtained in oblate bands are typically an order of magnitude larger [23]. For bands (2) and (3), only strong $M1$ transitions are observed, while the $E2$ crossover transitions are too weak to be observed in this experiment. These results show that much stronger $\Delta I = 1$ transitions relative to $\Delta I = 2$ transitions indeed exist in bands (2) and (3). Figure 6 shows plots of the moments of inertia J_1 of bands (2) and (3) in ^{141}Pm, the oblate bands in ^{136}La [3], ^{136}Ce [21], and ^{131}La [1], and the prolate bands in ^{134}Ce [22] and ^{132}Ba [23] against the rotational frequency $\hbar\omega$. From this figure, one can see that the moments of inertia J_1 of the bands (2) and (3) in ^{141}Pm are similar to those of oblate bands in ^{136}La, ^{136}Ce and ^{131}La, but are different from those of prolate bands in ^{134}Ce and ^{132}Ba. Figure 7 shows the plots of the staggering function of the level energies $[E(I) - E(I-1)]/2I$ against the spin I for bands (2) and (3) in ^{141}Pm. From this figure, one can see that signature splitting for bands (2) and (3) is small. The above analysis gives evidence for the oblate band assignments (with $\gamma \sim -60^\circ$) for bands (2) and (3) in ^{141}Pm.

For bands (4), (5), and (6) in ^{141}Pm, one can see that these bands have some characters similar to the oblate bands (2) and (3): (a) much stronger $\Delta I = 1$ transitions relative to $\Delta I = 2$ transitions inside the band; (b) moments of inertia are more similar to those of the oblate bands than those of the prolate bands, as shown in Fig. 8. However, another behavior in bands (4), (5), and (6) is different from the oblate bands; that is, large signature splitting occurs in these bands, as shown in Fig. 9. This type of band with large signature splitting based on high excitation energy has also been identified in neighboring nuclei [7,18], and was considered as the oblate-triaxial deformation with $\gamma \sim -90^\circ$. Based on the structural similarity, we assign bands (4), (5), and (6) in ^{141}Pm as oblate-triaxial deformation with $\gamma \sim -90^\circ$ also. In such deformation, the band structure not only shows the strong $M1$ transitions and the oblate moments of inertia, but also shows the large signature splitting caused by the triaxiality [18].

According to the excitation energies of band heads, bands (2)–(6) in ^{141}Pm probably belong to three or five quasiparticle bands, respectively. Thus, there may be many configurations to be selected for these bands. So to exactly determine the configurations of these high-spin bands is difficult. In order to understand the characters of these oblate bands in ^{141}Pm,

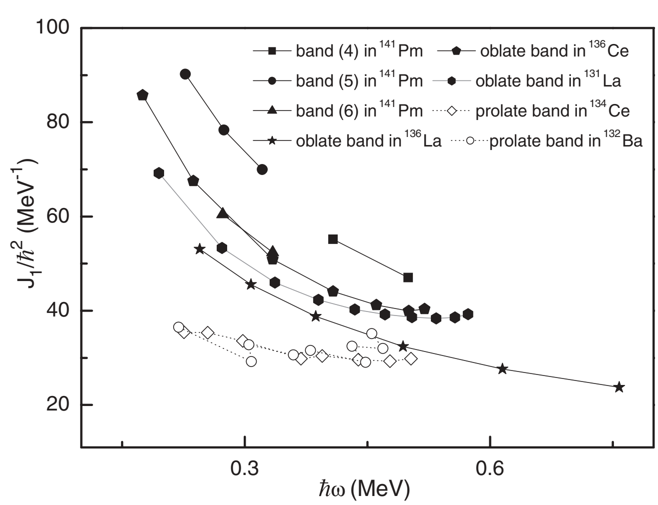

FIG. 8. Plots of the moments of inertia J_1 of bands (4)–(6) in ^{141}Pm, the oblate bands in ^{136}La, ^{136}Ce and ^{131}La, and the prolate bands in ^{134}Ce and ^{132}Ba against the rotational frequency $\hbar\omega$.

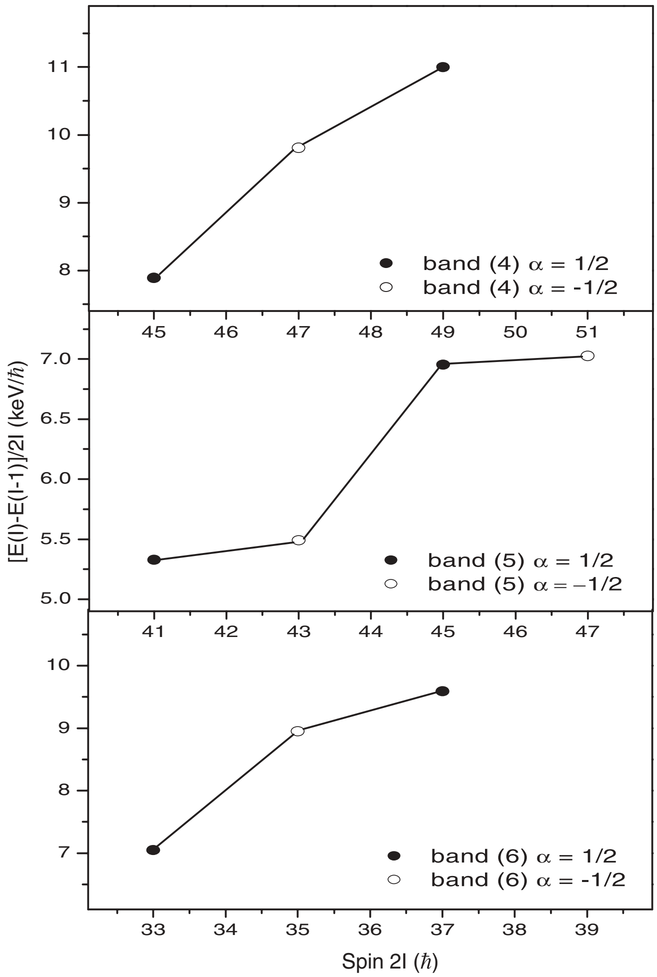

FIG. 9. Plots of the $[E(I) - E(I-1)]/2I$ vs the spin I for bands (4)–(6) in ^{141}Pm.

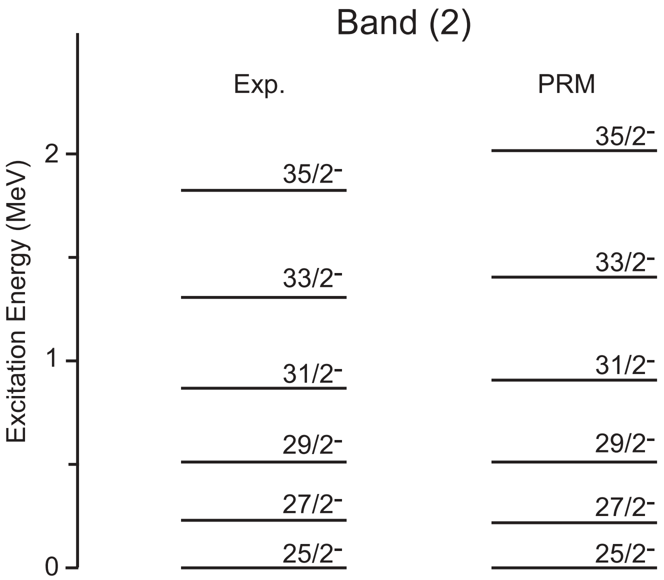

FIG. 10. The excitation energies from the PRM calculations in comparison with the experimental data of band (2) in ^{141}Pm.

we have carried out the triaxial n-particle-n-hole particle rotor model (PRM) calculations, in which more details can be seen in Ref. [24]. As a result, we only obtained the result of band (2). In the calculations, the coefficient of single-j Hamiltonian $C = 0.3$ MeV, which corresponds to the deformation parameter $\beta_2 = 0.22$, the triaxial deformation parameter $\gamma = 59^\circ$, and the moment of inertia parameter $\Im = 10$ MeV/$\hbar^2$. The calculations indicate that the quasiparticle configuration in band (2) is $\pi h_{11/2} \otimes (\nu h_{11/2})^2$. The calculated excited energy with the experimental data of band (2) in ^{141}Pm is shown in Fig. 10, where the excited energies of $25/2^-$ levels are set to be zero. From Fig. 10, one can see that the theoretical values of the excited energies are close to the experimental data. Thus, this calculated result suggests that band (2) has an oblate shape. The oblate shape in band (2) should originate from alignments of a pair of $h_{11/2}$ neutrons. On the other hand, in the calculations the deformation parameter $\beta_2 = 0.22$ is larger than the value of $\beta_2 = 0.15$ in the triaxial rotor plus particle model at the low-spin states taken by Aryaeinejad *et al.* [13] and Gülmez *et al.* [14]. This may indicate that not only strong oblate shape driving occurs, but strong β_2 shape driving occurs also at the high-spin states in ^{141}Pm. Unfortunately, for the other high-spin bands in ^{141}Pm, we cannot obtain satisfactory results from the calculations.

The clusters (A), (B), and (C) in Fig. 1 consist of some single particle levels and transitions. We cannot exactly determine the configurations, and more theoretical work is needed.

IV. SUMMARY

In the present work, the high-spin states of ^{141}Pm have been reinvestigated. The previous level scheme has been updated and many additional levels and transitions have been identified. Six collective band structures are observed. One band based on the $23/2^-$ state is suggested as the decoupled band, probably with a three quasiparticle configuration. Two collective bands based on $25/2^-$ and $35/2^-$ states are proposed as oblate deformation with $\gamma \sim -60^\circ$. Three other bands are proposed as oblate-triaxial deformation with $\gamma \sim -90^\circ$. The triaxial n-particle-n-hole particle rotor model calculations for one of the bands in ^{141}Pm are in good agreement with the experimental data, and suggest that this band may originate from the $\pi h_{11/2} \otimes (\nu h_{11/2})^2$ configuration with the oblate deformation. The other characteristics for the observed bands have been discussed.

ACKNOWLEDGMENTS

The work at Tsinghua University was supported by the National Natural Science Foundation of China under Grants No. 10975082 and No. 10775078, the Major State Basic Research Development Program under Grant No. 2007CB815005, and the Special Program of Higher Education Science Foundation under Grant No. 2010000211007. The authors wish to thank the staff of the in-beam γ-ray group and the tandem accelerator group at CIAE for their hospitality during the experiment and for providing the heavy-ion beam and the target.

[1] E. S. Paul *et al.*, Phys. Rev. Lett. **58**, 984 (1987).
[2] G. Andersson *et al.*, Nucl. Phys. A **268**, 205 (1976).
[3] S. J. Zhu *et al.*, Eur. Phys. J. A **24**, 199 (2005).
[4] S. J. Zhu *et al.*, Phys. Rev. C **62**, 044310 (2000).
[5] M. L. Li *et al.*, Phys. Rev. C **75**, 034304 (2007).
[6] Q. Xu *et al.*, Phys. Rev. C **78**, 034310 (2008).
[7] J. G. Wang *et al.*, J. Phys. G **37**, 125107 (2010).
[8] M. L. Li *et al.*, Eur. Phys. J. A **28**, 1 (2006).
[9] S. J. Zhu *et al.*, Chin. Phys. Lett. **16**, 635 (1999).
[10] G. Hackman *et al.*, Phys. Rev. C **47**, R433 (1993).
[11] A. Axelsson *et al.*, Eur. Phys. J. A **6**, 175 (1999).
[12] L. K. Peker, Nucl. Data Sheets **45**, 1 (1985).
[13] R. Aryaeinejad, P. M. Walker, R. B. Firestone, and W. C. McHarris, Phys. Rev. C **32**, 1855 (1985).
[14] E. Gülmez, M. W. Drigert, and J. A. Cizewski, Phys. Rev. C **39**, 1809 (1989).
[15] S. Bhattacharyya *et al.*, Nucl. Phys. A **730**, 23 (2004).
[16] D. C. Radford, Nucl. Instrum. Methods Phys. Res. A **361**, 297 (1995).
[17] C. W. Beausang, L. Hildingsson, E. S. Paul, W. F. Piel, N. Xu, and D. B. Fossan, Phys. Rev. C **36**, 1810 (1987).
[18] C. M. Petrache *et al.*, Nucl. Phys. A **603**, 50 (1996).
[19] C. W. Beausang, P. K. Weng, R. Ma, E. S. Paul, W. F. Piel, N. Xu, and D. B. Fossan, Phys. Rev. C **42**, 541 (1990).
[20] U. D. Pranmanik *et al.*, Nucl. Phys. A **632**, 307 (1998).
[21] E. S. Paul *et al.*, Phys. Rev. C **41**, 1576 (1990).
[22] S. J. Zhu *et al.*, High Energy Phys. Nucl. Phys. **29**, 130 (2005) (in Chinese).
[23] E. S. Paul, D. B. Fossan, Y. Liang, R. Ma, and N. Xu, Phys. Rev. C **40**, 1255 (1989).
[24] B. Qi *et al.*, Phys. Lett. B **675**, 175 (2009).